DEGREE PROJECT IN MATERIALS SCIENCE AND ENGINEERING, SECOND CYCLE, 30 CREDITS

*STOCKHOLM, SWEDEN 2021*

# Iron-catalyzed graphitization of biochar to produce graphitic carbon materials

**ZIYI SHI**

**KTH ROYAL INSTITUTE OF TECHNOLOGY**
**SCHOOL OF INDUSTRIAL ENGINEERING AND MANAGEMENT**

# Abstract

Demand for high-quality graphite is expected to experience an extraordinary growth rate, in large part due to its wide range of industrial applications such as adsorbents, lubricants, electrodes, etc. This thesis developed a novel sustainable approach to produce green-graphite materials by applying biochar, a carbon-rich valuable by-product obtained from biomass, as a carbon precursor. Meanwhile, iron-based catalysts are applied to enable the graphitization at a relatively lower temperature. This study focuses on the different parameters which could affect the evolution of carbon structure. The samples were mixed with catalyst in two ways, dry mixing and wet impregnation. Aside from the addition method, several parameters including temperature, heating duration, and iron loading amount were varied from 800 to 1300 ℃, 1 to 6 hours, and 0 to 33.6% respectively, to figure out an optimum graphitization process. The samples were characterized by X-ray diffraction, Raman scattering, SEM and particle size distribution analysis. Based on the characterization results, it was confirmed that with the increase of the graphitization temperature, duration and amount of iron loading, synthetic graphite performs a better graphitization and a higher conversion rate. Meanwhile, a detailed dissolution-precipitation mechanism was introduced and discussed in the context of iron-carbon equilibrium phase diagram to explain this catalytic process.



**Key words:** graphite, biochar, catalyst, catalytic graphitization

# Sammanfattning

Efterfrågan på högkvalitativ grafit förväntas uppleva en extraordinär tillväxttakt, till stor del på grund av dess breda utbud av industriella applikationer som adsorbenter, smörjmedel, elektroder etc. Denna avhandling utvecklade ett nytt hållbart tillvägagångssätt för att producera grön-grafitmaterial genom att applicera biokol, en kolrik värdefull biprodukt erhållen från biomassa, som en kolprekursor. Under tiden appliceras järnbaserade katalysatorer för att möjliggöra grafitisering vid en relativt lägre temperatur. Denna studie fokuserar på de olika parametrarna som kan påverka utvecklingen av kolstrukturen. Proverna blandades med katalysator på två sätt, torrblandning och våtimpregnering. Förutom tillsatsmetoden justeras flera parametrar, inklusive temperatur, uppvärmningstid och mängden järnbelastning för att få en optimal grafitiseringsprocess. Proverna karakteriserades genom röntgendiffraktion, Ramanspridning, SEM och partikelstorleksfördelningsanalys. Baserat på karakteriseringsresultaten bekräftades det att med ökningen av grafitiseringstemperaturen, varaktigheten och mängden järnbelastning, utför syntetisk grafit en bättre grafitisering och en högre omvandlingsfrekvens. Under tiden introducerades en detaljerad upplösnings-utfällningsmekanism och diskuterades i sammanhanget av järn-kol-jämviktsfasdiagrammet för att förklara denna katalytiska process.



**Nyckelord**: grafit, biokol, katalysator, katalytisk grafitisering

# Table of Contents

1. Introduction ..... 1
    1.1. Problems from synthetic graphite manufacturing ..... 1
    1.2. Objectives ..... 3
2. Graphitization: from carbon precursor to graphite ..... 4
    2.1. Graphite ..... 4
    2.2. Biomass ..... 6
    2.3. Catalyst ..... 6
3. Methodology ..... 9
    3.1. Overall process ..... 9
    3.2. Experiemnt setup ..... 9
        3.2.1 Preparation ..... 9
        3.3.1. X-ray diffraction (XRD) ..... 11
        3.3.2. SEM and EDS ..... 11
        3.3.3. Particle size distribution ..... 12
        3.3.4. Raman scattering ..... 12
4. Result and discussion ..... 13
    4.1. X-ray diffraction (XRD) ..... 13
    4.2. Raman scattering ..... 20
    4.3. Particle size distribution ..... 22
    4.4. SEM and EDS ..... 23
    4.5. Catalytic graphitization mechanism ..... 24
    4.6. Reflection on social and ethical ..... 27
5. Conclusions ..... 28
6. Recommendations for future work ..... 29
7. Acknowledgement ..... 31
8. References ..... 32

# 1. Introduction

## 1.1. Problems from synthetic graphite manufacturing

Graphite, as a crystalline allotrope of carbon material where the carbon atoms arrange in a hexagonal structure, has already attracted considerable interest for many industrial applications due to some impressive merits, such as low thermal expansion, excellent thermal shock resistance, high chemical stability, and high thermal conductivity [1, 2]. It is a naturally occurring mineral extracted from metamorphic rocks or igneous rocks in which some sedimentary carbon compounds are reduced [3]. However, since only a few countries dominate natural sources of mined graphite around the world, graphite has been labeled as 'supply risk' material and becomes one of the major global concerns. To fill the gap between supply and demand, in 1893, Charles Street of Le Carbone developed the first industrial process for synthetic graphite. In the mid-1890s, Edward Goodrich Acheson came up with another approach to produce artificial graphite by synthesizing carborundum, which identifies that carborundum at high temperature can be converted into almost pure graphite. This study provides foundation for modern large-scale production of synthetic graphite, which help reducing dependency toward nature mineral [4].

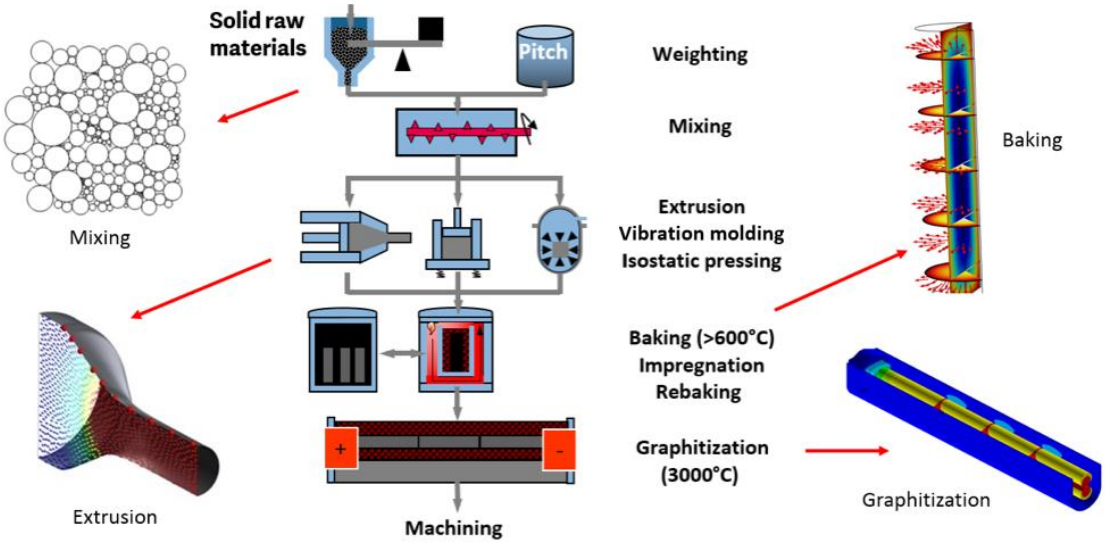


**Fig. 1** Schematic diagram for industrial process of artificial graphite [5]

A schematic diagram for the manufacturing process of the artificial bulk graphite is shown in Fig. 1. It contains a series of mechanical processes and heat treatment are involved for purification of graphite. Basically, soft carbons obtained from fossil fuels like coal, petroleum and heavy oils, are used for

artificial graphite production [6]. After blending and grinding coke and pitch to fine particles, these raw materials are further extruded, compressed and molded by several mechanical processes. Following carbonization undergoes between 700 and 1200 ℃, in which organic compounds are decomposed into carbon stacked in a roughly parallel pattern with stochastic orientation. To achieve complete graphitization, temperature is further raised to around 2750 ℃ to enable transformation of graphitic crystallite, requiring a long period time over 1 day. Therefore, one problem emerged from this manufacturing process is the resource shortage of fossil fuel and the rise of environmental pressure. It indicates that there is an increasing need for graphite industry to decrease usage of fossil fuel and energy demand to the lowest limit, developing to a green sustainable artificial graphite process.

Biomass, a sustainable carbon-rich material, has been regarded as a promising substitute to replace fossil fuel for graphitization due to its abundant availability [7, 8]. A number of research results indicate a great feasibility of using waste biomass resources to produce graphitize electrodes via a series processes based on catalytic graphitization, acid washing and shaping [9]. Compared with biomass, biochar is a solid byproduct obtained from pyrolysis which is a thermal decomposition process for biomass occurred in a protective gas atmosphere producing bio-oil, biogas, and biochar. Biochar contains large amount of unconverted carbonaceous residues that is commonly used as soil amendments and to produce functionalized carbon materials [10, 11]. In recent years, more research shift focuses on biomass and biochar due to high utilization potential to replace char and pitch in graphite industry.

Graphitization temperature is one of most vital factors determining the degree of graphitization. If temperature cannot fulfil the specific requirement, the graphitic structure will not be completely developed, which refers to the materials consist of graphitic crystallite and turbostratic quasicrystalline [12]. Previous studies also pointed out that involvement of catalyst is one of most effect approaches to decrease lowest graphitization heat temperature, achieving lower energy consumption. Krivoruchko et.al. presented that, with the aid of catalyst, graphitization temperature can be lowered to a minimum of 600 ℃ [13]. Differed from traditional artificial graphite synthesis method which involves two steps of heat treatment, carbonization and graphitization, catalytic graphitization can be conducted in one-step, directly converting amorphous carbon to high-quality graphite. Thereby, taking into account the energy cost for graphite synthesis, it is considered as one of the most feasible and sustainable methods.

## 1.2. Objectives

In this work, a cascaded biorefinery process of catalytic graphitization to produce green graphite powders from biochar is proposed. A comprehensive and systematic study of the iron-based catalyst, graphitization temperature, duration and addition method are conducted. The aim of the study is to: 1) to conduct a comprehensive review of the evolution of amorphous carbon; 2) to develop a sustainable, low carbon emission cascaded biochar biorefinery process for green graphite powders production; 3) to investigate best parameters for synthesis process to benchmark against the commercial graphite powders production process.

# 2. Graphitization: from carbon precursor to graphite

## 2.1. Graphite

Graphite, also referred to plumbago or black lead, is a mineral which has a hexagonal layered structure consisting of rings of six carbon atoms arranged in widely spaced parallel sheets with an -ABAB- stacking sequence [14]. Carbon atoms in ring arrays are in the sp2-hybridized state where the bond length is 0.142 nm. In the sp2 carbon network model, each carbon atom is bonded to three other carbon atoms. Each layer of graphite is linked by weak van der Waals bonds, and the distance between planes is 0.335 nm. The schematic structure of graphite is shown in Fig. 2. Additionally, there is also another graphite structure called Rhombohedral or Beta graphite which can be introduced as a stacking fault of hexagonal graphite, -ABCABC- stacking sequence as shown in Fig. 3, in microstructure. Due to its thermodynamic instability, Rhombohedral graphite can only be found in combination with hexagonal graphite, but never in pure form. This unstable structure tends to revert to hexagonal stacking by processing heat treatment above 1600°C or increase by conducting proportion.

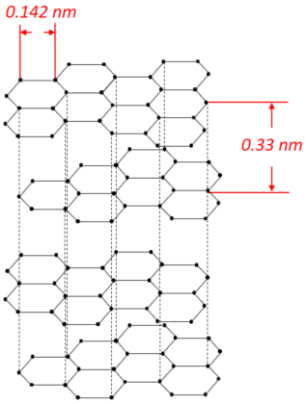


**Fig. 2** Diagram for ideal hexagonal graphite showing an -ABABAB- stacking sequence.

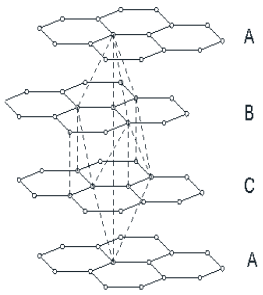


**Fig. 3** Diagram for ideal rhombohedral graphite.

As the bonding force between graphene layers is much weaker than that of intra layers, graphite can be easily modified along basal planes, leading to another form of graphite, turbostratic graphite, as illustrated in Fig. 4. It is generally regarded as a variant of standard graphite (hexagonal graphite). In both structures, the graphene layers are stacked up with a regular spacing, but the difference is the stacking ordering degree. Compared with hexagonal graphite consisted of an ordered AB stacking structure, the graphene layers of turbostratic graphite are randomly translated to each other and rotated about the normal of graphene layers, performing a different interlayer spacing. However, in some experiments, curvature and local positive fluctuation of interlayer spacing of graphene layers were also observed and included in turbostratic graphite. In comparison with hexagonal graphite (pure graphite) where the interlayer spacing ($d_{002}$) is 0.3354 nm, ($d_{002}$) of turbostratic graphite characterized by X-ray diffractometry (XRD) is between 0.340 and 0.344 nm, depending on the translation distance or rotation degree [15]. However, it should be mentioned that the ($d_{002}$) obtained from XRD is an average value varying with the degree of conversion between turbostratic graphite and hexagonal graphite.

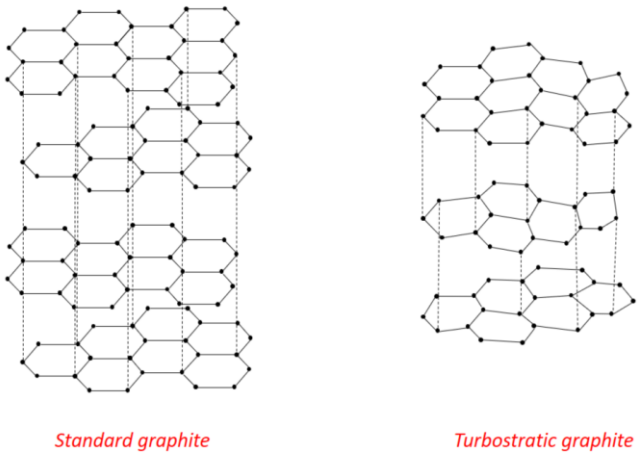


**Fig. 4** Diagram for turbostratic graphitic and standard graphite

To properly quantify the comparison of interlayer spacing in graphite and degree of conversion from turbostratic graphite to standard graphite, 'degree of graphitization' is introduced as an index [16]. The closer the lattice size is to the point constant of the ideal graphite, the higher the degree of graphitization. An empirical formula called Maire and Merings equation is applied to calculate the degree of graphitization:

$$g = \left(\frac{0.344 - d_{002}}{0.0086}\right) * 100\% \quad (1)$$

where 0.344 nm is the maximum interlayer spacing of turbostratic stacking. and 0.0086 nm is the difference between maximum interlayer spacing and interlayer spacing for pure graphitic stacking.

### 2.2. Biomass

Biomass refers to a renewable organic material that comes from plants and animals. The usage of biomass for transportation and for electricity generation is steadily increasing in many developed countries, which is regarded as an effective means of avoiding greenhouse gas emissions from fossil fuel [11, 17]. Therefore, as a carbon-rich material, it is quite promising to substitute coke or pitch to synthesize artificial graphite.

Generally, biomass can be categorized into three types of polymers, including cellulose $(C_6H_{10}O_5)_n$, hemicellulose $(C_5H_8O_4)_m$ and lignin $[C_9H_{10}O_3(OCH_3)_{(0.9-1.7)}]_n$ [18]. A large amount of research has been done to investigate the feasibility and effectiveness of graphitization of plant-based biomass. Jiang Deng et al. found that XRD patterns for artificial graphite derived from lignin performed a narrower peak at 24° which is closer to pure graphite reflection peak 26.55° than those samples yielded from cellulose or hemicellulose, revealing its higher degree of graphitization [19]. In addition, their conclusion further stated that the high carbon content of final chars yielded from lignin with the highest thermal stability was the major contributor to a better graphitization. Biochar is a solid byproduct containing unconverted carbonaceous residues. It can be extracted by pyrolysis which is a thermal decomposition process for biomass in an oxygen-free atmosphere, producing bio-oil, biogas, and biochar. In comparison with lignin where carbon accounts for around 60%, biochar typically reach over 90% [10]. Thereby, in recent years, more and more research shift focus to biochar due to its better potential to replace char and pitch in graphite industry.

### 2.3. Catalyst

Catalytic graphitization is defined as a chemical reaction between carbonaceous precursor and catalysts to form graphite materials [20]. A number of articles have demonstrated that the addition of catalyst will enhance carbon crystallinity, further improving the efficiency of overall graphitization [21]. The kinetic mechanism of the acceleration is negative free energy for the conversion from amorphous atomic structure to graphitic atomic structure, which is directly reflected on the decrease of the heat treatment temperature needed for graphitization [22]. For non-graphitizable raw material, with the help

of catalyst, the graphitization can be achieved at a minimum of 600℃ [13]. Thus, it is considered a promising method to cut energy consumption during graphite synthesis.

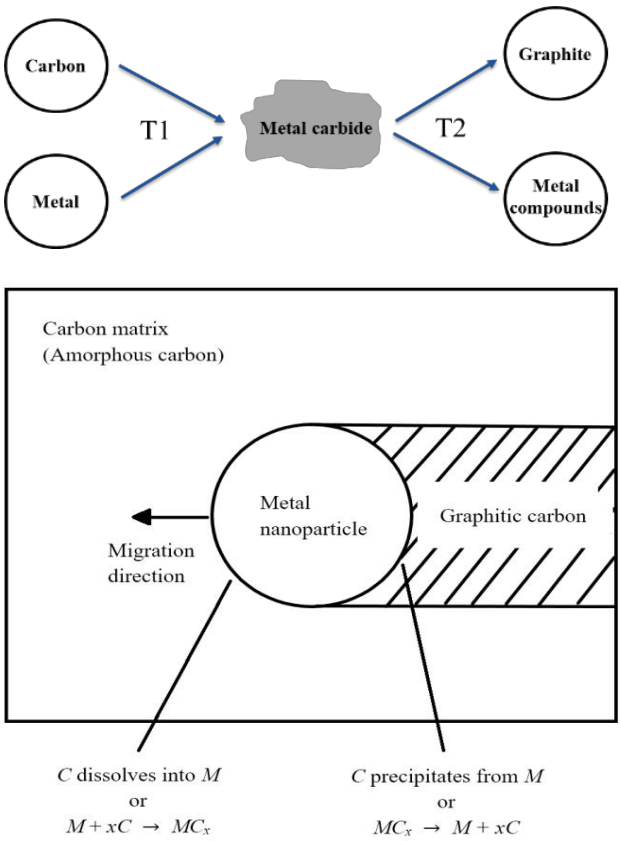


**Fig. 5** Diagram for two mechanisms of catalytic graphitization.

Currently, some transition metals such as V, Zr, Pt, Ti, Al, Mn, Fe, Co, Ni and metallic compound $Cr_2O_3$, $MnO_2$, $MnO_3$, $Fe_3O_4$ commonly act as catalysts in graphitizing the amorphous carbon materials [23]. Theoretically, in these catalyst metals, Fe, Co, Ni and Mn perform better influence as catalyst owning to the electrons in d-shell orbitals, resulting in strong chemical bonds between metal and carbon, which further contributes to more active metal carbides [24]. Sevalla et al once carried out a graphitization experiment and confirmed that Fe, Ni and Co are effective catalyst in graphite production [25]. Based on the conclusion, Hoekstra and his team investigated the effect of different Iron salt composition on graphitized cellulose. Three catalysts, iron (III) nitrate, ammonium iron (III) citrate and iron (III) chloride were employed in the experiment. They proposed that the extent of graphitization is determined by the properties of iron salt, specifically whether the catalyst is included as non-volatile iron salt [22]. It is due to that different type of iron salts influences textural properties of carbonaceous precursor to further determine their graphitic structure, and non-volatile iron salt is a better option than volatile one.

Two mechanisms behind catalytic graphitization of amorphous carbon to graphitic carbon have been proposed [24], as outlined in Fig. 5. One is the dissolution-precipitation, whereby amorphous carbon in the matrix firstly dissolves into metal nanoparticles, followed by precipitation as graphitic carbon. Another one is the metal carbide formation-decomposition. Amorphous carbon firstly reacts with metal nanoparticles to form a carbide intermediate, which is under metastable state at a specific temperature. The intermediate will then decompose into the metal and graphitic carbon. However, it cannot give an explanation to the formation of turbostratic graphite. It is found that turbostratic graphite tends to be produced in the sample system where the metal catalyst particles are homogenously distributed with a size of around 20 um [26]. Further investigation and experiments should be conducted to develop a new mechanism in which the formations of hexagonal graphite and turbostratic graphite are combined together.

# 3. Methodology

## 3.1. Overall process

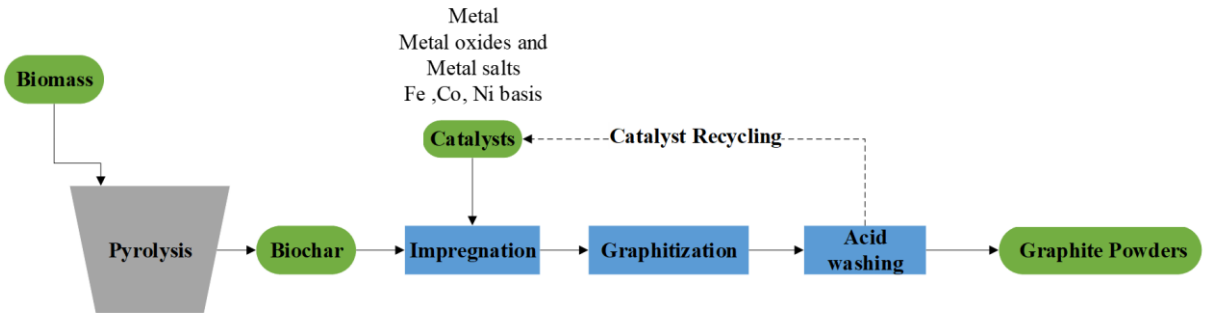


**Fig. 6** Flow chart for the designed manufacturing process of green graphite.

In this work, a new graphite synthesis process was developed based on biomass as starting point in Fig. 6. Firstly, biomass pyrolysis was conducted at a temperature range of 500-800°C by using softwood as raw material. According to previous literature review, after comprehensive consideration of factors, including toxicity, economics and catalyst behavior, iron (III) nitrate and pure iron is utilized as catalyst in our work. To ensure a homogenous contact between catalyst species and feedstock, the solid product, biochar, were further impregnated or physically mixed with the Iron (III) nitride or Iron particle.

For both two addition ways, mixtures of biochar and catalyst were put into an electrical furnace for catalytic graphitization with protective gas at a temperature in a range of 800-1300 °C for a period time of 1-6 hours with a fixed heat rate. After the high temperature heat treatment, double acid washing was carried out to remove catalyst in the graphite. Also, the filtrate containing ferric ion ($Fe^{3+}$) was collected and the liquid was vaporized at a temperature around 90 ºC to recycle catalysts. The recycling efficiency are calculated according to the ratio of catalyst amount recycled-to-catalyst amount input.

After each step, samples will be dried and analyzed for ash and iron content. Removal efficiency of each acid will be calculated according to the iron content decrease. Final obtained graphite products were then characterized by using XRD, Raman spectrum, SEM, EDS, and particle size distribution (PSD) analyzer.

## 3.2. Experiemnt setup

3.2.1 Preparation

The biochar supplied by Envigas AB (Stockholm, Sweden) was used as carbonaceous precursor for the catalytic synthesis of graphite materials. It was produced from softwood pyrolysis at the temperature of 550℃. The elemental analysis of the biochar issued by Eurofin is shown in Table. 1. It contains an abundant carbon content of approximately 91 wt%.

**Table. 1** Elemental analysis of the biochar.

| Proximate analysis | Sample |
|---|---|
| | Biochar |
| C-fix (% dw) | 90.12 |
| Ash content (% dw) | 2.08 |
| Ultimate analysis (% dw) | |
| C | 91.4 |
| H | 2.6 |
| N | 0.22 |
| O* | 3.6 |
| S | <0.011 |
| Cl | 0.0036 |

To prepare artificial graphite, iron (III) nitrate ($Fe(NO_3)_3 \cdot 9H_2O$, analytical grade) was mixed in deionized water (300 mL) in mass ratios of 0, 11.2%, 22.4% and 33.6%. Each mixture was stirred at room temperature by magnetic stirrer until it became a metal/biochar paste. In additional to wet impregnation, the biochar was physically mixed with iron particle and iron (III) nitrate respectively in mass ratio of 22.4%. Subsequent graphitization of the composite was carried out in a tubular furnace under nitrogen atmosphere. The oven-dried mixture was placed in a corundum crucible and heated at 800℃, 1100℃ and 1300℃ for 1, 3 and 6 hours with a heating rate of 15℃/min, under nitrogen atmosphere (200 ml/min). After heating, the sample was collected after natural cooling to room temperature. The graphitized samples thus obtained were washed with 1 mol/L aqueous $HNO_3$ and copious deionized water under ultrasonic vibration to eliminate the metal particles that were remained after the graphitization. The samples were put into a glass bottle containing certain amount of Aqua regia solution and heated for a temperature of 120 °C for 2 hours. The final products, obtained in powder form, were then oven-dried at 100 °C for 24 h. All treated samples after removing the metal particles are

denoted as G-X-Y-Z-A-B in Table. 2, where X is the graphitization temperature, Y is the mass ratio of iron (III) nitrate to biochar, Z is heating time, A is addition method and B is catalyst composition.

**Table. 2** Details of samples prepared for graphitization.

| Sample name | Temperature (℃) | Loading amount ratio (%) | Time (h) | Addition method | Catalyst |
|---|---|---|---|---|---|
| G-800-11.2-3h-WET-FENO | 800 | 11.2 | 3 | Wet impregnation | $Fe(NO_3)_3 \cdot 9H_2O$ |
| G-1100-11.2-3h-WET-FENO | 1100 | 11.2 | 3 | Wet impregnation | $Fe(NO_3)_3 \cdot 9H_2O$ |
| G-1300-11.2-1h-WET-FENO | 1300 | 11.2 | 1 | Wet impregnation | $Fe(NO_3)_3 \cdot 9H_2O$ |
| G-1300-11.2-3h-WET-FENO | 1300 | 11.2 | 3 | Wet impregnation | $Fe(NO_3)_3 \cdot 9H_2O$ |
| G-1300-11.2-6h-WET-FENO | 1300 | 11.2 | 6 | Wet impregnation | $Fe(NO_3)_3 \cdot 9H_2O$ |
| G-1300-22.4-3h-WET-FENO | 1300 | 22.4 | 3 | Wet impregnation | $Fe(NO_3)_3 \cdot 9H_2O$ |
| G-1300-33.6-3h-WET-FENO | 1300 | 33.6 | 3 | Wet impregnation | $Fe(NO_3)_3 \cdot 9H_2O$ |
| G-1300-22.4-3h-DRY-FENO | 1300 | 22.4 | 3 | Dry mixing | $Fe(NO_3)_3 \cdot 9H_2O$ |
| G-1300-22.4-3h-DRY-FE | 1300 | 22.4 | 3 | Dry mixing | Fe |

## 3.3. Characterization

3.3.1. X-ray diffraction (XRD)

XRD patterns of biochar and samples were obtained on a Bruker D8 Advance diffractometer using Cu-Kα1 radiation (λ = 0.154056 nm). Data were collected between 10° and 80° at a scanning speed of 0.02 °/s. The interlayer spacing ($d_{002}$) of each sample was calculated by applying Bragg's equation to the (002) diffraction peak, $d_{002} = \lambda / 2\sin\theta$ [27]. And the parameter (g) expressing the degree of graphitization of the carbon material was obtained by applying the equation,

$$g = \left(\frac{0.344 - d_{002}}{0.0086}\right) * 100\% \quad (1)$$

The average crystallite size ($L_c$) in the layer stacking direction was evaluated from the diffraction peak for the (002) plane by applying the Scherrer formula [28],

$$L_c = \frac{0.9\lambda}{\beta\cos\theta} \quad (2)$$

Where β is FWHM in radians.

3.3.2. SEM and EDS

SEM observation is carried out by S3700N Hitachi SEM (20 kV and 10 mm working distance) with the back scattered electrons (BSE) signal. EDS Mapping scanning was implemented to assess the residual amount and distribution of catalyst after acid washing.

3.3.3. Particle size distribution

The textural properties of the biochar and samples were determined through low temperature nitrogen adsorption isotherms at 77K using a Micromeritics ASAP 2000 11 instrument. All the samples were degassed under vacuum at 150°C before each measurement. The surface area was calculated based on the Brunauer-Emmett-Teller (BET) model, and the micropore surfaces were measured by applying the t-plot method.

3.3.4. Raman scattering

Raman test is conducted by Tyrode I at Department of Chemistry in KTH. The first-order Raman spectrum is characterized by two peaks: disorder-induced peak (D-band) at wavelength around 1350 $cm^{-1}$ and the graphite peak (G-band) at around 1580 $cm^{-1}$. To quantify the quality of artifical graphite mateirals, α value is introduced in this work, which is expressed as follows:

$$\alpha\,\% = \frac{I_G}{I_G + I_D} * 100 \tag{3}$$

where $I_G$ and $I_D$ represent the intensity of D-band and G-band respectively.

# 4. Result and discussion

Heat treatment of catalyst-treated biochar to 800, 1100 and 1300 ℃ with 1, 3 and 6 hours under nitrogen yielded black solid in the form of fine powders. Averagely, a 10 g sample of biochar produced around 4 g of graphitic carbon product. The photograph of the synthetic graphite impregnated with 22.4 wt% iron loading and processed at 1300℃ for 3 hours is shown in Fig. 7.

**Fig. 7** Photograph of the graphite graphitized at 1300℃ for 3 h with 22.4 wt% loading.

### 4.1. X-ray diffraction (XRD)

X-ray Diffraction (XRD) is the most common experimental method determining the atomic and molecular structure of carbon materials, in which the crystalline structure causes a beam of incident X-rays to diffract into some specific directions. First, in order to get rid of the effect of temperature on the biochar without catalyst, raw material and biochar heated at 1300 ℃ without catalyst are both analysed by XRD, shown in Fig. 8. In the XRD diagram, there are the broad peaks at 25° and 42°, which indicates a considerable amount of highly amorphous carbon atoms. Both samples perform similar position and intensity of the board peaks, attributed to that graphitization of biochar cannot be achieved below 1300 ℃ without catalyst.

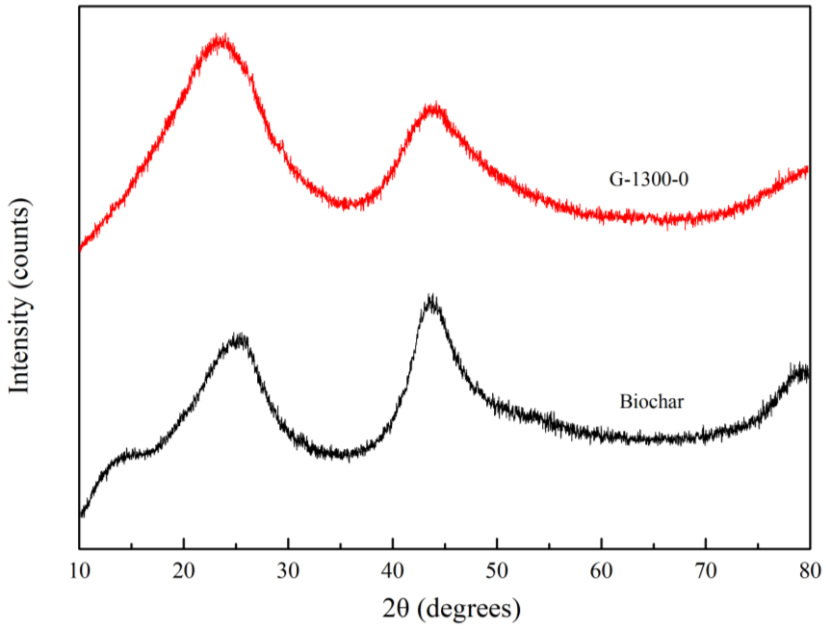


**Fig. 8** XRD patterns for the biochar and the sample treated at 1300℃ without catalyst.

After catalytic graphitization, the XRD patterns of the processed samples are consistent with graphite with no evidence of any other phases. The most distinct difference among these patterns is the position of the most intensive peak which represents the degree of graphitization. Fig. 9 shows the XRD patterns for the samples catalytically graphitized at 800, 1100, and 1300 ℃ for 3 hours with 11.2%. Fig. 10 shows the samples treated at 1300 ℃ for 1, 3 and 6 hours with 11.2%. Due to the effective catalytic behaviour on feedstock, those samples perform five strong diffraction peaks in XRD patterns which are quite different form raw materials. The five peaks correspond five planes, (002), (100), (101), (004), and (110) in the order of the peak position. Among these planes, (002) is the strongest peak, and the intensities of other peaks are relatively weak. Fig. 11 shows the schematic lattice planes of (002), (100), (101), and (110) in an ideal graphite crystal. Based on the diagram, in additional to (002) depicting a graphene layer, the integrity of the (100), (101), and (110) planes is influenced by the stacking of graphene layers, implying the rotation and translation of graphene can bring a significant effect on the (100), (101), and (110) planes. Therefore, the detailed information of (002) peak is usually involved to evaluate the quality of graphene layer.

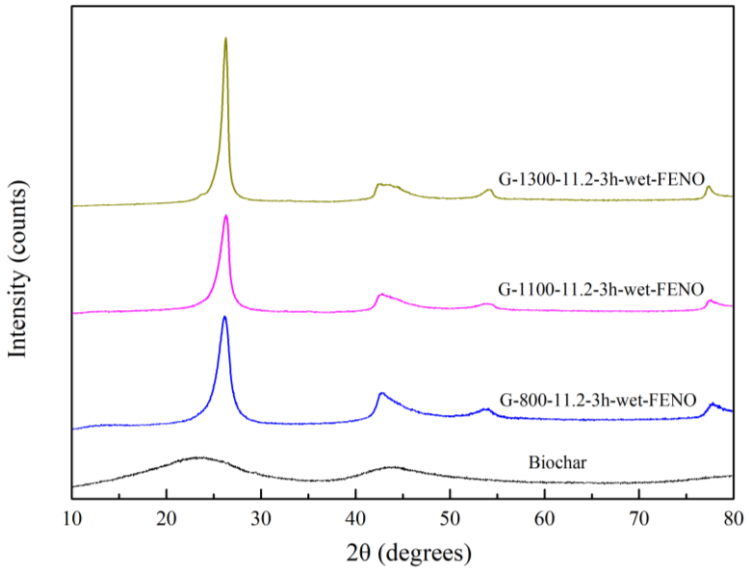


**Fig. 9** XRD patterns for the samples graphitized at different temperatures for 3 h with 11.2 wt% loading.

Some phenomena and results can be obtained based on the analysis of XRD patterns in Fig. 9. They directly reflect that: (i) Because of the growth of the size of graphite crystallite in the $L_c$ with the increase of temperature, the (002) and (004) peaks go sharper than other peaks, indicating a larger FWHM value. (ii) With the increase of temperature, the shape of the (101) peak becomes more obvious, which could be indexed as a better stacking of graphene with less rotation and translation. (iii) The peak for the (110) plane becomes narrower with the increase of temperature, indicating a growth of the size of graphite crystallite in the $L_a$ direction.

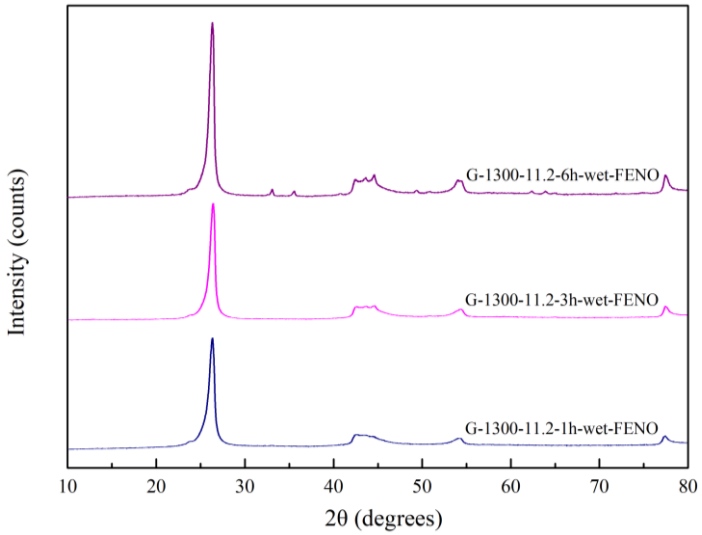


**Fig. 10** XRD patterns for the samples graphitized at 1300 ℃ for different graphitization time with 11.2 wt% loading.

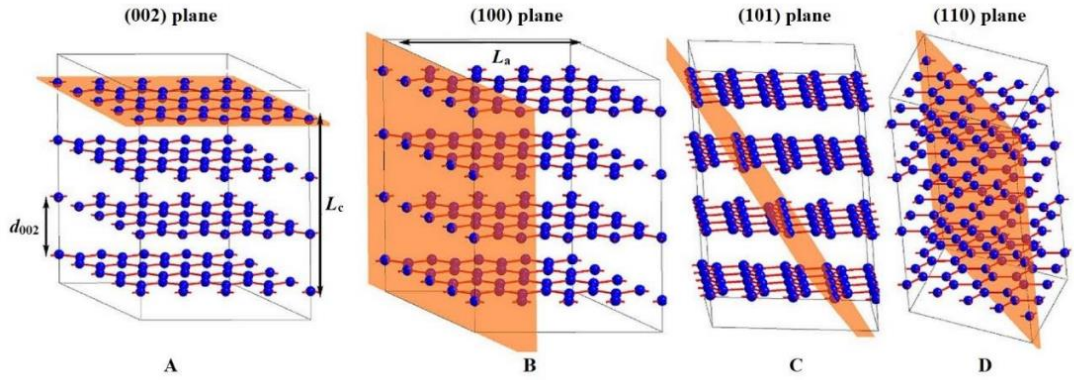


**Fig. 11** Schematic diagrams of (002), (100), (101), and (110) lattice planes in the ideal graphite crystal.

Fig. 12 shows the XRD patterns for the samples processed at 1300°C for 3 hours with loading amount of 11.2%, 22.4% and 33.6%. Fig. 13 is the XRD patterns for the samples with different addition methods and catalyst. Overall, three trends mentioned before can also be observed in Fig. 13, revealing that the amount of catalyst loading plays a predominant role in improving the growth of graphite lattice and the stacking of graphene. The sample physically mixed with Iron powder has strongest (002) peak among the three products. Aside from the intensity of peaks, after selecting the interval from 24 to 28 in the XRD patterns, all the (002) peaks shows different degrees of shift to the standard peak position of pure graphite. As the positions of turbostratic graphite and hexagonal graphite are 25.8° to 26.2° [12] and 26.55° respectively. It is concluded that these samples contain both carbon structures whose peaks overlap with each other to form a broad peak region between 26.2° and 26.55°. The position shift of (002) peak demonstrates that less amorphous carbon were consumed and more graphitic carbon were produced during graphitization with the increase of the graphitization temperature, graphitization time and catalyst loading amount.

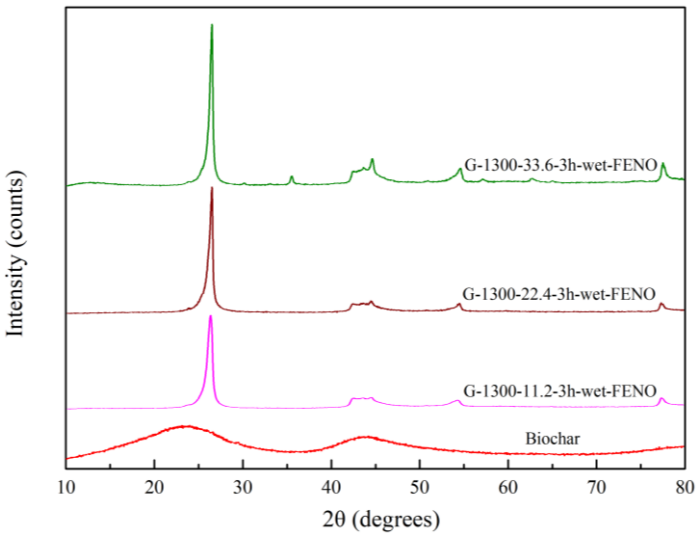


**Fig. 12** XRD patterns for the samples graphitized at 1300 ℃ for 3h with different loading.

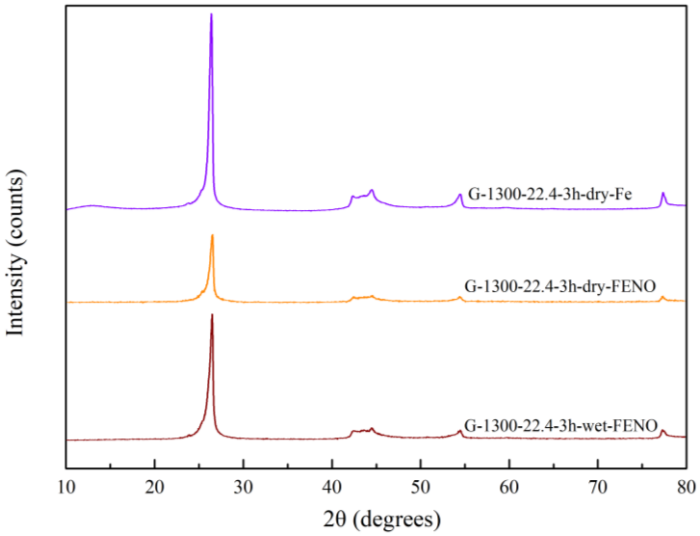


**Fig. 13** XRD patterns for the samples graphitized at 1300 ℃ for 3h with different addition methods.

In this work, the interlayer spacings ($d_{002}$) and the crystallite size ($L_c$) of the samples and the degree of graphitization (G%) are introduced to quantity the catalytic influence of catalyst type, addition method, heating time and heating temperature on the carbon structural evolution. Three parameters were calculated and summarized in Table. 3 based on Fig. 14. The parameters of commercial graphite and pure graphite are attached in this table as well.

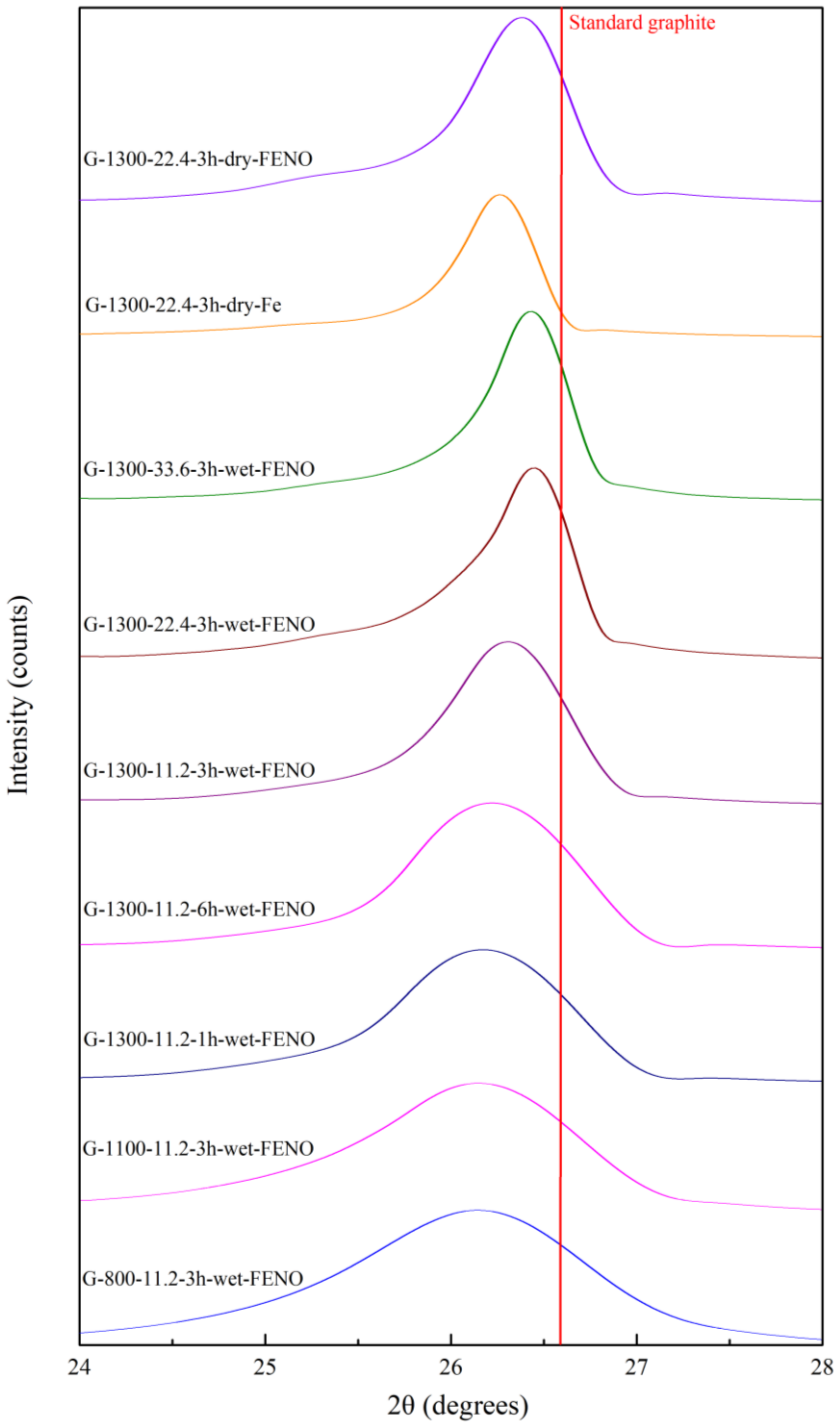


**Fig. 14** XRD patterns in the interval from 24° to 28° for all samples.

The degree of graphitization for different samples is plotted in Fig. 15**.** The catalyst loading amount, heating time and heating temperature are positively correlated with the degree of graphitization, showing that the promotion effect of iron nitride and wet impregnation is very remarkable. The $d_{002}$ value of the sample, G-1300-22.4-WET-FENO, is quite smaller than other treated samples, and its g% value is as high as 91.32%, indicating that the graphitic structure in this sample is very close to pure graphite and

much better than commercial graphite. With the increase of temperate and time, the $L_c$ value performs an upward trend. But the mechanism of the largest $L_c$ of sample, G-1300-22.4-3h-DRY-FENO, should be considered in future.

**Table. 3** Details of samples prepared for graphitization.

| Sample name | $d_{002}$ (nm) | G (%) | $L_c$ (nm) |
|---|---|---|---|
| G-800-11.2-3h-WET-FENO | 0.3406 | 39.10 | 5.26 |
| G-1100-11.2-3h-WET-FENO | 0.3407 | 38.43 | 6.27 |
| G-1300-11.2-1h-WET-FENO | 0.3397 | 50.32 | 10.45 |
| G-1300-11.2-3h-WET-FENO | 0.3382 | 68.00 | 11.82 |
| G-1300-11.2-6h-WET-FENO | 0.3376 | 73.85 | 12.55 |
| G-1300-22.4-3h-WET-FENO | 0.3361 | 91.32 | 16.00 |
| G-1300-33.6-3h-WET-FENO | 0.3363 | 89.03 | 18.54 |
| G-1300-22.4-3h-DRY-FENO | 0.3364 | 88.42 | 18.56 |
| G-1300-22.4-3h-DRY-FE | 0.3387 | 62.11 | 17.36 |

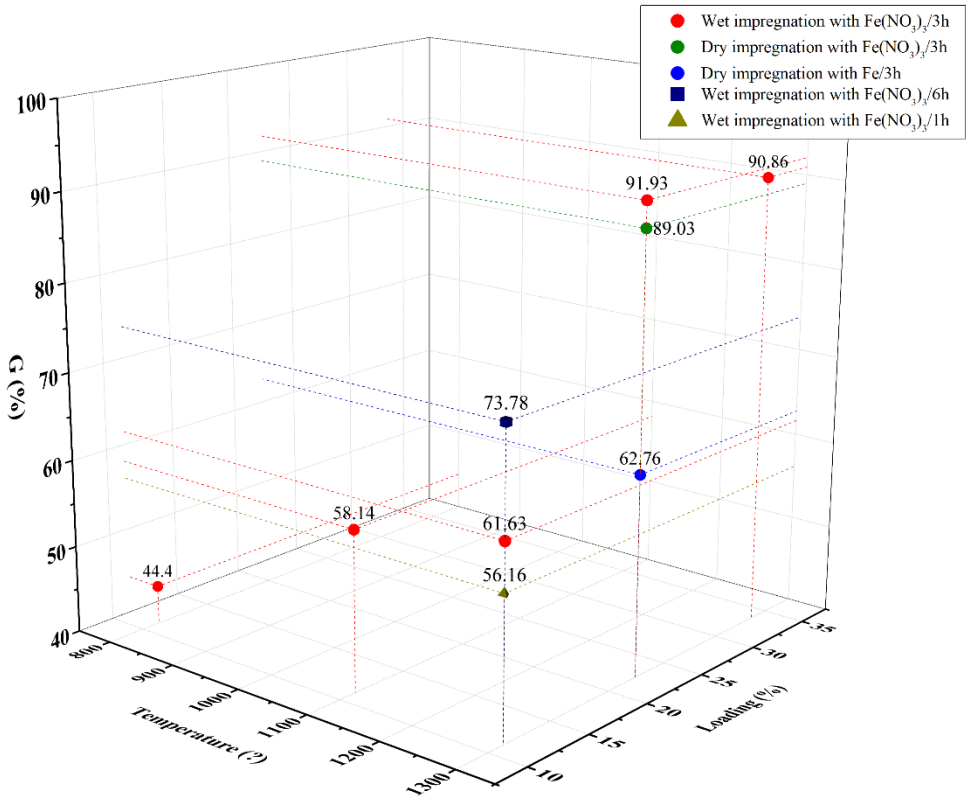


**Fig. 15** The summary of degree of graphitization for all samples.

## 4.2. Raman scattering

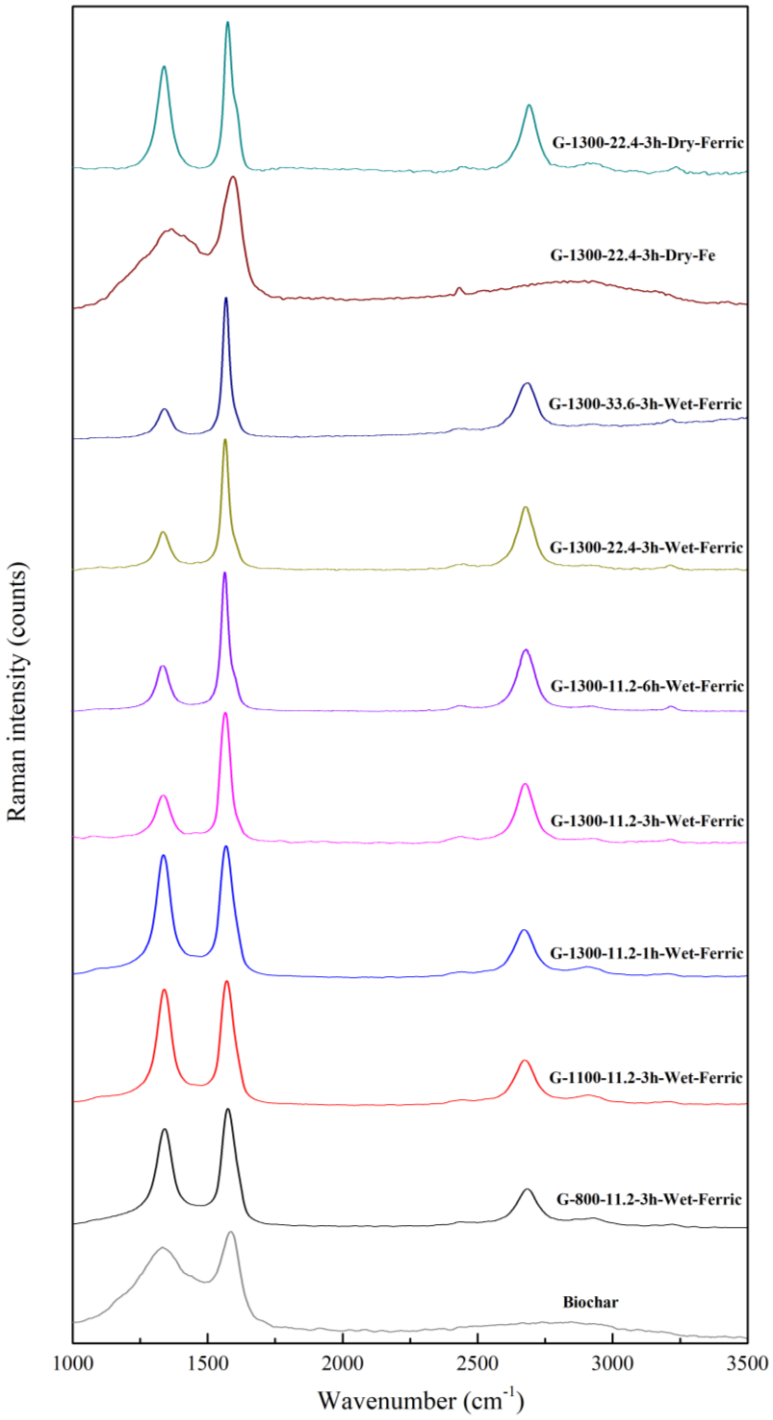


**Fig. 16** Raman patterns for all samples.

The Raman spectra of graphitized sample derived from biochar with different parameters is shown in Fig. 16. The first-order Raman spectrum is characterized by two peaks: disorder-induced peak (D-band) at wavelength around 1350 $cm^{-1}$ and the graphite peak (G-band) at around 1580 $cm^{-1}$. The intensity of D-peak and G-peak are related to the ordering of the graphitic structure. The α value, calculated on the

basis of the intensity value of D-band and G-band, is a measure of the degree of order where higher ratio indicates lower disorder and higher amounts of graphite. The specific conversion rate (α) is listed in Table. 4. It should be noticed that the α value of G-1300-33.6-3h-WET-FENO is 82.81%, which implies that the presence of a catalyst promotes the reordering of the carbon structure at lower temperature. Another evidence of the graphitic structure can be found in the broad band around 2700 $cm^{-1}$. This band is a result of second order resonance from the D band, and can be called the G′, 2D or D* band which is characteristic of stacked graphene layers [29]. The results show that when the catalyst was added to biochar via wet impregnation method, the increase of the graphitization temperature, catalyst loading, and the graphitization duration time all induce an increase of α. Moreover, whether the catalyst is $Fe(NO_3)_3$ or Fe powder, when it is added to biochar via the dry impregnation method using optimal process parameters, produced graphite powders exhibit much lower α compared to the G-1300-22.4-WET-3h-FENO. Therefore, a well contact between catalyst and biochar seems also to be essential for a better conversion from disordered carbon to graphitic carbon. Among all the produced graphite powders, the graphite powder with the maximum g%, i.e. G-1300-22.4-WET-3h-FENO, also has relatively high $L_c$ and α values. Though G-1300-33.6-WET-3h-FENO was proven to have slightly higher α and slightly larger crystallize stacking height, a higher catalyst loading could increase the difficulty for catalyst removal. Therefore, in this study, G-1300-22.4-WET-3h-FENO powder was regarded as the optimal sample and used for graphite electrodes production and related characterization.

**Table. 4** Details of samples prepared for graphitization.

| Sample name | α |
|---|---|
| G-800-11.2-3h-WET-FENO | 56.16 |
| G-1100-11.2-3h-WET-FENO | 74.54 |
| G-1300-11.2-1h-WET-FENO | 51.09 |
| G-1300-11.2-3h-WET-FENO | 62.61 |
| G-1300-11.2-6h-WET-FENO | 76.95 |
| G-1300-22.4-3h-WET-FENO | 78.38 |
| G-1300-33.6-3h-WET-FENO | 82.81 |
| G-1300-22.4-3h-DRY-FENO | 59.85 |
| G-1300-22.4-3h-DRY-FE | 61.51 |

### 4.3. Particle size distribution

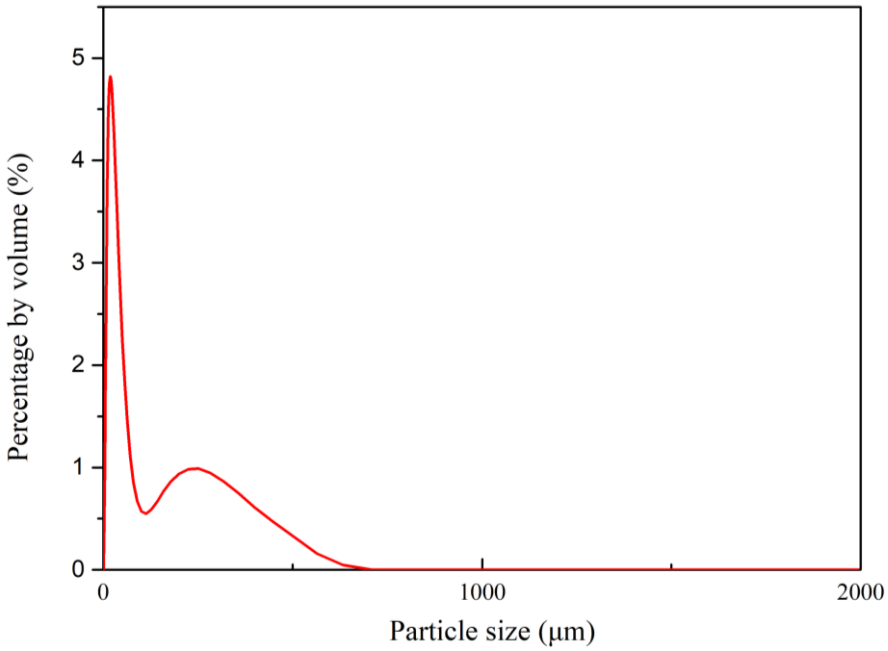


**Fig. 17** Particle size distribution of sample of G-1300-22.4-3h-wet-FENO

Particle size is a unique parameter to quantify meaningfully for some forms of carbon material. In the case of synthetic flake graphite, the particle size is relatively easy to determine, i.e. the diameter of the sphere. Fig. 17 displays the particle size distribution of optimal graphite sample G-1300-22.4-3h-WET-FENO. The results show that this sample have more concentrated distribution than other commercial graphite. The average particle size (D50) of sample is 18 μm, which means that there is less specific surface area for the formation of solid electrolyte interphase layer. Therefore, this artificial graphite is proper for graphite anode in lithium-ion batteries.

**Table. 5** PSD analysis results of the optimal sample.

| Sample | Particle size (um) | | |
|---|---|---|---|
| | D10 | D50 | D90 |
| Graphite | 5.064 | 18.009 | 96.415 |
| AGP-818 (commercial graphite) | 10-13 | 18-20 | 55 |

### 4.4. SEM and EDS


**Fig. 18** SEM image of sample of G-1300-22.4-3h-wet-FENO

SEM images of artificial graphite, G-1300-22.4-WET-3h-FENO reveals that 10−20 μm diameter plate-like graphite materials are homogeneously distributed on the matrix. In Fig. 18, most flakes are ~15 μm wide and ~5 μm thick. In fact, the morphology of G-1300-22.4-3h-WET-FENO graphite flakes look very similar to commercial artificial graphite produced from biomass. From the SEM micrographs of materials, the distribution of particle sizes is consistent with results obtained from particle size distribution analysis.

Despite the benefits of a high amount of iron loading, it can also lead to excessive iron residues that are difficult to remove completely. The mapping scan of EDS in Fig. 19 reveals the presence of iron particles attaching the graphite, implying that nitric acid washing cannot exactly remove catalyst from the final products. This is probably due to that iron particles are embedded into the graphite shells, leading to a low contact area between iron and acid.

After nitric acid washing, graphite sample was further washed using Aqua regia under microwave digestion. In Fig. 20, there is no Fe particles observed on graphite matrix, presenting residual catalyst is completely removed. This image is in good agreement with the result obtained from XRD spectrum.

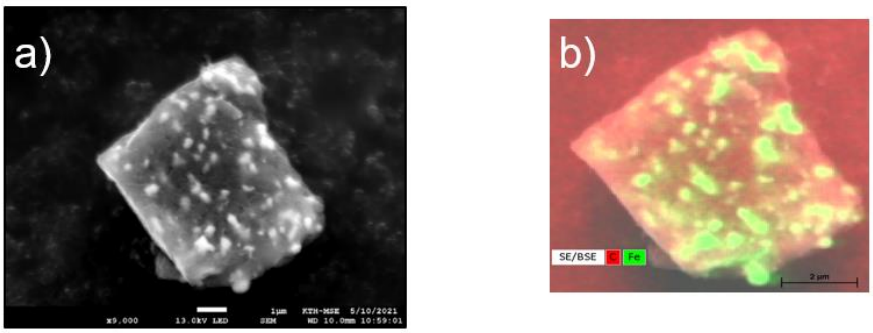


**Fig. 19** a) SEM image of G-1300-22.4-3h-wet-FENO after nitric acid washing; b) EDS mapping scan image of G-1300-22.4-3h-wet-FENO after nitric acid washing

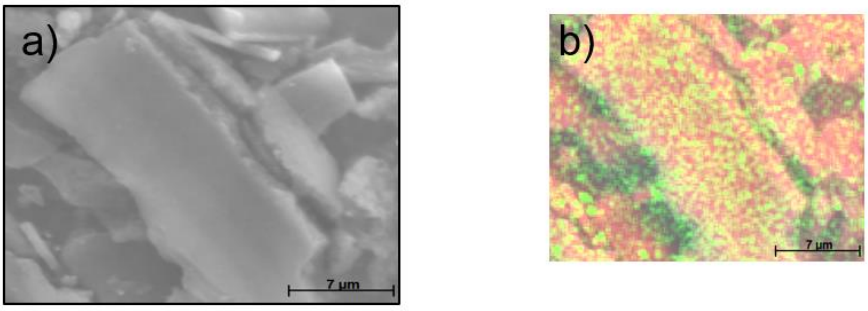


**Fig. 20** a) SEM image of G-1300-22.4-3h-wet-FENO after Aqua regia washing; b) EDS mapping scan image of G-1300-22.4-3h-wet-FENO after Aqua regia washing

### 4.5. Catalytic graphitization mechanism

In this study, the range of catalyst ratio is 0, 11.2, 22.4 and 33.6%. Based on dissolution-precipitation mechanisms for catalytic graphitization mentioned above, a postulated growth model illustrated in Fig. 21 can be introduced to explain the formation of graphite encapsulated iron nanoparticles. Taking G-1300-22.4-3h-WET-FENO as an example, the decomposition of iron precursor into $\alpha$ -$Fe_2O_3$ during drying is involved as the first stage. After the formation of $\alpha$ -$Fe_2O_3$, the biochar and iron oxide mixture are annealed at around 1000 ℃ in which most of the oxygen functional groups, such as $H_2$, CO, $CO_2$ and $H_2O$, are evaporated from the biochar matrix. In this step, the iron reduction process can occur by the existence of gaseous phases like CO and $H_2$ rather than reaction with solid carbon material. According to the iron-carbon phase diagram (Fig. 22) at a temperature of 1300 ℃, due to the unpaired electron affinity between 2p of C and 3d of Fe, α-Fe in carbon matrix will be converted to γ-Fe. As the carbon atoms start dissolving, the gaps that exist between the iron atoms of face centered cubic (fcc) can

be fitted into by these atoms at 1000 ℃.

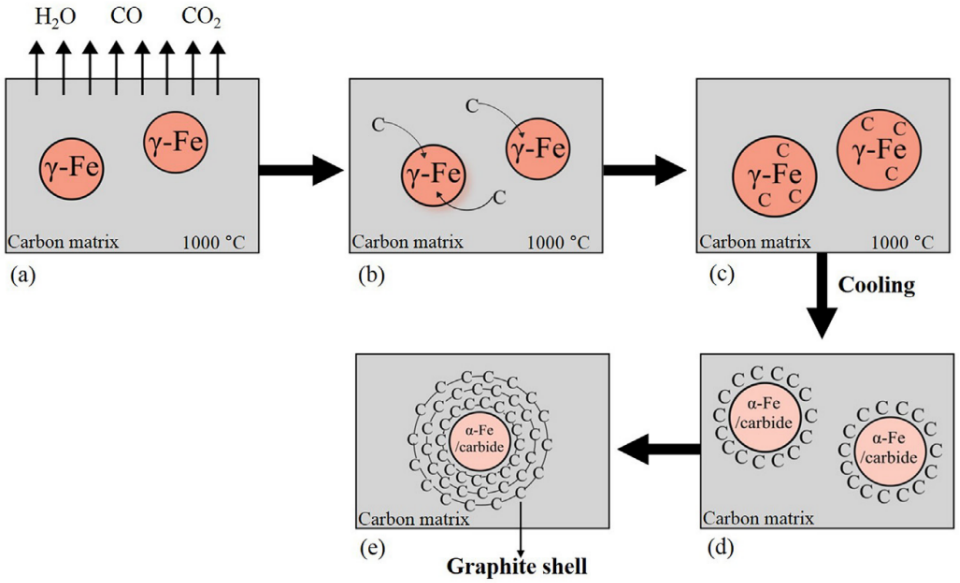


**Fig. 21** Schematic illustration of evolution of carbon encapsulated iron core-shell nanoparticles.[30]

However, the solubility of carbon in iron is limited at 4.6% when temperature is increased to 1300 ℃. When the carbon content in the multiphase exceed the solubility limit 4.6% (supersaturation state), the excess carbon atoms are aggregated into a new discrete $Fe_3C$ phase, resulting in the precipitation of some excess carbon in the form of graphitic carbon over the metallic iron nanoparticles surface, which is called encapsulation process. On the basis of the formation of the first graphite layer, additional graphitic layers are formed sequentially between the original sheet and the iron particle. Furthermore, it is possible to make a thermodynamic assessment to the formation of graphitic multilayer encapsulation of iron nanoparticles through the Molecular Dynamics (MD) simulations proposed by Feng Ding et al [31].

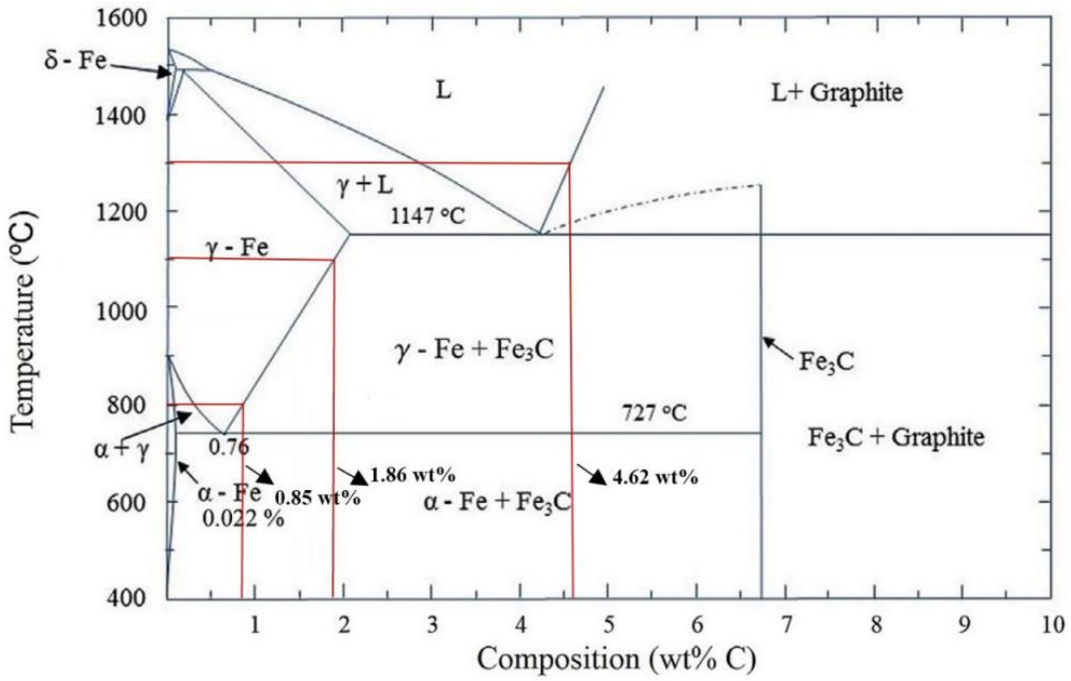


**Fig. 22** Iron-carbon equilibrium phase diagram

In addition to adjusting catalyst content, catalytic graphitization was observed at temperatures of 800, 1100, and 1300°C and different heating time of 1h, 3h, and 6h. As mentioned before, graphite can be form either by dissolution-precipitation from the catalyst or by the evolution of graphitic nanostructure through self-ordering process at ultra-high temperature. From the former theory, the temperature and heating time effect might occur since catalyst particles nucleate and grow into larger size as heating temperature increasing. At higher temperature upon heating process, catalyst particle will quickly grow with considerable size, good crystallinity, and good dispersion that can facilitate the formation of graphitic nanostructure layers [32]. Compared with temperature, longer graphitization time can provide considerable time for the growth of catalyst particles. This explains why the catalytic effect of iron is more remarkable at higher temperature and longer heating time.

Also the results shows that, compared to traditional catalyst addition method, the wet impregnation approach could realize a better phase transformation from amorphous structure to graphitic structure at same temperature. As iron nitride in solution has a smaller particle size than iron particle, applying wet impregnation with iron nitride can achieve a homogenous distribution in carbonaceous precursor matrix, further yielding better artificial graphite.

### 4.6. Reflection on social and ethical

From social aspect, catalytic graphitization technology can satisfy 17 sustainable development goals proposed by United Nations. As mentioned before, the implementation of biochar and catalyst can dramatically reduce environmental pressures, which exactly meets the requirement of GOAL 7: Affordable and Clean Energy. Specifically, the novel graphitization process will enhance energy efficiency and promote the investigation on cleaner fossil-fuel technology.

From ethical aspect, there is no visible potential negative effect on ethical of this study so far. This study presents a comprehensive and systematic understanding of the mechanism of graphitization behaviours, letting the industrial community has a better assess achieve real application of catalytic graphitization according to the fundamental parameters study in this work.

# 5. Conclusions

A sustainable manufacturing process to produce green graphite materials is proposed in this work. In the comparison with the traditional industrial synthesis method, renewable biochar and iron nitride were employed as the carbonaceous precursor and catalyst respectively in this novel graphitization process to lower the graphitization temperature from 2500°C to 1300°C. Artificial graphite materials with a high degree of graphitization were successfully synthesized by conducting heat treatment to the mixture. This work has proved that the conversion from amorphous carbon to graphitic structure is dependent on several factors including graphitization temperature, graphitization time, addition method and amount of iron catalyst loading. XRD patterns of samples treated with different conditions indicated that longer graphitization time, higher graphitization temperature and larger amount of iron loading result in a better degree of graphitization, larger size of graphitic crystallite and higher conversion rate from amorphous carbon to graphite.

Based on the analysis data of XRD and Raman patterns, the optimal process parameters for catalytic graphitization are determined. The sample, G-1300-22.4-3h-WET-FENO, that was processed at 1300°C for 3h with 22.4 wt% iron nitride catalyst loading, performs best ordered graphitic layer structure where the average crystallite size, the degree of graphitization and α are 16.00 nm, 91.32% and 78.38% respectively. To better understand the development of graphitic structure, the mechanism of the influence of graphitization temperature, time, addition method and catalyst type was discussed via involving nucleation theory, SEM analysis diagram and iron-carbon phase diagram. To overcome the biggest obstacle, the residue of iron catalyst in graphite matrix, a new acid washing method was developed to remove the iron by applying Aqua regia under microwave digestion, further achieving widespread industrial applications. Meanwhile, compared to commercial graphite whose values are 21 nm, 100% and 0.1, there is a great improvement potential for the quality of the synthetic graphite. And to refine the catalytic graphitization process, hybrid catalyst, biomass carbonaceous precursor and stepwise heating are put forward as chief research subjects in next step.

# 6. Recommendations for future work

Although a graphite material with a high degree of graphitization (91.86%) has been successfully synthesized using catalytic graphitization from the biochar, some innovation points are quite worth to explore:

1. Evaluating the Hybrid catalyst on the catalytic graphitization process

Hybrid catalyst, including two or more types of metals, has also been proven to be more efficient. Lan major et.al proposed a new Fe-Co hybrid catalyst for catalytic graphitization of miscanthus grass powders. It is found that implementing hybrid catalyst, multi metal complexes or clusters were formed during heat treatment due to the combination of different metal and these compounds exhibit a higher catalytic activity, compared with single catalyst. As a result, the graphitization efficiency was doubled compared to process using single iron or cobalt as catalyst. The result means that the energy consumption and $CO_2$ emission during graphitization are dramatically less than traditional industrial graphite synthesis process. Therefore, developing novel hybrid catalyst i.e., transition metal alloys, or transition metal and rare earth metal alloys seems to be a promising way to maximize the graphitization process. Notably, manganese has been reported to exhibit a similar graphitization effect with cobalt at same heating temperature, but a high sensitivity to acid makes it easier to be removed afterwards than cobalt and other transition metals. Combing all above mentioned information, a Fe-Mn based hybrid catalyst is of great significance to study.

2. Investigating effect of type of carbon precursor on the catalytic graphitization process.

Different raw materials, such as sawdust and lignin from paper and pulping industries can be chosen in future work. Biochar will be firstly produced via pyrolysis of biomass, and different properties biochar with different compositions, surface areas and different carbon fixed will be obtained. These different carbon precursors will be further impregnating with catalyst, then proceed further for different temperature, then following removing catalyst by acids washing. Obtained graphite will be evaluated to qualify the potential of usage of different raw materials.

3. Stepwise heating

Particle size of the catalyst has also been recognized as one essential factor for the quality, especially the crystal properties of the graphite products. It was generally acknowledged that, in order to obtain

graphite with highly regular crystal structure, the particle size of the catalyst need to be greater than a certain value. Catalyst with particle size lower than this number mainly promote turbostratic carbon production. However, a relatively big particle size of catalyst is not conductive for the contact between catalyst and biochar. A premixing of fine-particle-size catalyst and biochar for inmate contact and promoting the growth of catalyst particles before graphitization represents a promising solution. Therefore, a stepwise heating process is suggested.

# 7. Acknowledgement

I would like to thank my supervisors, Docent Weihong Yang, post-doc Tong Han and PhD students Shule Wang, Yuming Wen and Hanmin Yang from Department of Materials Science and Engineering at KTH for their strong support, enthusiastic encouragement, creative ideas, and valuable criticism on this thesis project. I would also like to thank every member of the group for their advice and help.

I would like to express my gratitude to all the faculty members of the Department of Materials Science and Engineering at KTH Royal Institute of Technology who helped me during my two years of Master's studies.

Envigas AB is acknowledged for supplying the biochar.

I also thank all my family and Yage who gave me the best love during this time!

# 8. References


[1] H. O. Pierson, *Handbook of carbon, graphite, diamonds and fullerenes: processing, properties and applications*. William Andrew, 2012.

[2] B. T. Kelly, "Physics of graphite," 1981.

[3] R. B. Cook, "Handbook of Mineralogy," *Rocks and Minerals,* vol. 76, no. 4, p. 278, 2001.

[4] S. Ragan and H. Marsh, "Science and technology of graphite manufacture," *Journal of materials science,* vol. 18, no. 11, pp. 3161-3176, 1983.

[5] B. Jokanović, in *Optimizing Thermal Processes in Carbon Manufacturing with Simulation*, ed. COMSOL, 2018.

[6] S.-M. Lee, D.-S. Kang, and J.-S. Roh, "Bulk graphite: materials and manufacturing process," *Carbon letters,* vol. 16, no. 3, pp. 135-146, 2015.

[7] P. McKendry, "Energy production from biomass (part 1): overview of biomass," *Bioresource technology,* vol. 83, no. 1, pp. 37-46, 2002.

[8] Y. M. Bar-On, R. Phillips, and R. Milo, "The biomass distribution on Earth," *Proceedings of the National Academy of Sciences,* vol. 115, no. 25, pp. 6506-6511, 2018.

[9] Z. Wang, D. Shen, C. Wu, and S. Gu, "State-of-the-art on the production and application of carbon nanomaterials from biomass," *Green Chemistry,* vol. 20, no. 22, pp. 5031-5057, 2018.

[10] T. Kan, V. Strezov, and T. J. Evans, "Lignocellulosic biomass pyrolysis: A review of product properties and effects of pyrolysis parameters," *Renewable and Sustainable Energy Reviews,* vol. 57, pp. 1126-1140, 2016.

[11] J. Deng, M. Li, and Y. Wang, "Biomass-derived carbon: synthesis and applications in energy storage and conversion," *Green chemistry,* vol. 18, no. 18, pp. 4824-4854, 2016.

[12] G. Nover, J. B. Stoll, and J. von Der Gönna, "Promotion of graphite formation by tectonic stress–a laboratory experiment," *Geophysical Journal International,* vol. 160, no. 3, pp. 1059-1067, 2005.

[13] O. P. Krivoruchko, N. I. Maksimova, V. I. Zaikovskii, and A. N. Salanov, "Study of multiwalled graphite nanotubes and filaments formation from carbonized products of polyvinyl alcohol via catalytic graphitization at 600–800 C in nitrogen atmosphere," *Carbon,* vol. 38, no. 7, pp. 1075-1082, 2000.

[14] B. McEnaney, "Structure and bonding in carbon materials," *Carbon Materials for advanced technologies,* pp. 1-34, 1999.

[15] A. Ōya, M. Mochizuki, S. Ōtani, and I. Tomizuka, "An electron microscopic study on the turbostratic carbon formed in phenolic resin carbon by catalytic action of finely dispersed nickel," *Carbon,* vol. 17, no. 1, pp. 71-76, 1979.

[16] F. Maldonado-Hódar, C. Moreno-Castilla, J. Rivera-Utrilla, Y. Hanzawa, and Y. Yamada, "Catalytic graphitization of carbon aerogels by transition metals," *Langmuir,* vol. 16, no. 9, pp. 4367-4373, 2000.

[17] P. Basu, *Biomass gasification, pyrolysis and torrefaction: practical design and theory*. Academic press, 2018.

[18] S. V. Vassilev, D. Baxter, L. K. Andersen, and C. G. Vassileva, "An overview of the chemical composition of biomass," *Fuel,* vol. 89, no. 5, pp. 913-933, 2010.

[19] J. Deng, T. Xiong, H. Wang, A. Zheng, and Y. Wang, "Effects of cellulose, hemicellulose, and lignin on the structure and morphology of porous carbons," *ACS Sustainable Chemistry & Engineering,* vol. 4, no. 7, pp. 3750-3756, 2016.

[20] M. Demir *et al.*, "Graphitic biocarbon from metal-catalyzed hydrothermal carbonization of lignin," *Industrial & Engineering Chemistry Research,* vol. 54, no. 43, pp. 10731-10739, 2015.

[21] X. Wu, K. Chen, Z. Lin, Y. Zhang, and H. Meng, "Nitrogen doped graphitic carbon from biomass as non noble metal catalyst for oxygen reduction reaction," *Materials Today Energy,* vol. 13, pp. 100-108, 2019.

[22] J. Hoekstra *et al.*, "The effect of iron catalyzed graphitization on the textural properties of carbonized cellulose: Magnetically separable graphitic carbon bodies for catalysis and remediation," *Carbon,* vol. 107, pp. 248-260, 2016.

[23] J. Hoekstra, A. M. Beale, F. Soulimani, M. Versluijs-Helder, J. W. Geus, and L. W. Jenneskens, "Base metal catalyzed graphitization of cellulose: a combined Raman spectroscopy, temperature-dependent X-ray diffraction and high-resolution transmission electron microscopy study," *The Journal of Physical Chemistry C,* vol. 119, no. 19, pp. 10653-10661, 2015.

[24] A. Ōya and H. Marsh, "Phenomena of catalytic graphitization," *Journal of Materials Science,* vol. 17, no. 2, pp. 309-322, 1982.

[25] M. Sevilla and A. B. Fuertes, "Catalytic graphitization of templated mesoporous carbons," *Carbon,* vol. 44, no. 3, pp. 468-474, 2006.

[26] M. Johnson and K. Faber, "Catalytic graphitization of three-dimensional wood-derived porous scaffolds," *Journal of Materials Research,* vol. 26, no. 1, pp. 18-25, 2011.

[27] Z. Zhang and Q. Wang, "The new method of XRD measurement of the degree of disorder for anode coke material," *Crystals,* vol. 7, no. 1, p. 5, 2017.

[28] A. Patterson, "The Scherrer formula for X-ray particle size determination," *Physical review,* vol. 56, no. 10, p. 978, 1939.

[29] I. Major, J.-M. Pin, E. Behazin, A. Rodriguez-Uribe, M. Misra, and A. Mohanty, "Graphitization of Miscanthus grass biocarbon enhanced by in situ generated FeCo nanoparticles," *Green Chemistry,* vol. 20, no. 10, pp. 2269-2278, 2018.

[30] S. T. Neeli and H. Ramsurn, "Synthesis and formation mechanism of iron nanoparticles in graphitized carbon matrices using biochar from biomass model compounds as a support," *Carbon,* vol. 134, pp. 480-490, 2018.

[31] F. Ding, A. Rosen, E. E. Campbell, L. K. Falk, and K. Bolton, "Graphitic encapsulation of catalyst particles in carbon nanotube production," *The Journal of Physical Chemistry B,* vol. 110, no. 15, pp. 7666-7670, 2006.

[32] F. Jiang *et al.*, "Ultrahigh-temperature conversion of biomass to highly conductive graphitic carbon," *Carbon,* vol. 144, pp. 241-248, 2019.

TRITA ITM-EX 2021:464